Sensors & Actuators: B. Chemical 309 (2020) 127760

Contents lists available at ScienceDirect

Sensors and Actuators B: Chemical

journal homepage: www.elsevier.com/locate/snb

Surface plasmon resonance amplified efficient polarization-selective volatile organic compounds CdSe-CdS/Ag/PMMA sensing material

Ming-Chung Wu[a,b,c,*], Chih-Kunag Kao[a], Tz-Feng Lin[d], Shun-Hsiang Chan[a,b], Shih-Hsuan Chen[a], Chi-Hung Lin[a], Yu-Ching Huang[e], Ziming Zhou[f], Kai Wang[f], Chao-Sung Lai[e,g,h,i,**]

[a] Department of Chemical and Materials Engineering, Chang Gung University, Taoyuan, 33302, Taiwan
[b] Green Technology Research Center, Chang Gung University, Taoyuan, 33302, Taiwan
[c] Division of Neonatology, Department of Pediatrics, Chang Gung Memorial Hospital, Linkou, Taoyuan, 33305, Taiwan
[d] Department of Fiber and Composite Materials, Feng Chia University, Taichung, 40724, Taiwan
[e] Department of Materials Engineering, Ming Chi University of Technology, New Taipei City, 24301, Taiwan
[f] Department of Electrical & Electronic Engineering, South University of Science and Technology of China, Shenzhen, 518055, Guangdong, China
[g] Department of Electronic Engineering, Chang Gung University, Taoyuan, 33302, Taiwan
[h] Biosensor Group, Biomedical Engineering Research Center, Chang Gung University, Taoyuan, 33302, Taiwan
[i] Department of Nephrology, Chang Gung Memorial Hospital, Linkou, Taoyuan, 33305, Taiwan

ARTICLE INFO

Keywords:
Volatile organic compounds
Sensor
Quantum rods
Electrospinning
Polarization-selective
Surface plasmon resonance

ABSTRACT

Volatile organic compounds (VOCs) are potentially dangerous to the environment and human health. The developed sensing template in this study was prepared by a one-step process on a glass substrate using the electrospinning technique. The sensing material made of the uniaxial aligned CdSe-CdS/Ag/PMMA composite scaffold consists of CdSe-CdS core-shell quantum rods, silver nanoparticles (Ag NPs), and poly(methyl methacrylate) (PMMA) nanofibers. Increasing the specific surface area is beneficial for VOCs harvesting; therefore, the uniaxial aligned CdSe-CdS/Ag/PMMA composite scaffold was slightly treated with UV-ozone etching, and thus efficiently enhancing the extinction changes of VOCs. Also, a high VOC detection capability was demonstrated by the polarization response and Ag surface plasmon resonance of the nanocomposite. A series of typical VOCs and alcoholic VOCs were used for the VOCs sensor practical tests. This VOC sensor achieved a spectacular detection limit of 100 ppm for butanol and 500 ppm for chlorobenzene. The uniaxial aligned CdSe-CdS/Ag/PMMA composite scaffold is a newly designed nanocomposite and can reach the market demands comparing to other commercial high sensitive VOC sensors.

1. Introduction

Volatile organic compounds (VOCs) cause severe to fatal accidents in fire or explosion when the vapor concentration of chemicals meets the lowest explosion limit. It is thus essential to develop gas sensors as precautionary tools to prevent any potential risk in storage, in transportation, and the use of VOCs. A useful VOC sensor should be designed as a sensor with real-time detection, high sensitivity, and high reproducibility [1–5]. Liu et al. fabricated p-type NiO nanoparticles to detect 100 ppm VOCs with high response [6]. Paknahad et al. reported that the microfluidic-based gas detector exhibited high selectivity for 1000 ppm VOCs [7]. Kim et al. proposed the Pt- and Pd-decorated ZnO nanowires for 50 ppm toluene and 50 ppm benzene detection [8].

Recently, many types of gas sensors have attracted attention, such as acoustic sensor [9], metal oxide semiconductor sensor [10], and transistor sensor [11]. Although these types of sensors show excellent sensitivity and detection limits, they also present some challenges. The preparation of surface acoustic wave sensors requires vacuum deposition equipment or metal oxide targets, which increases equipment costs [12]. Metal oxide semiconductor sensors require high-temperature processes [13]. The fabrication process of the field-effect transistor device is cumbersome, and gold is often used as an electrode [14]. Optical sensors are a potential research area because the preparation of sensing materials is relatively simple. Without the need for a multilayer device structure, it only requires a substrate and sensing material [15]. The preparation process can even use a full solution process [15–17].

A variety of sensing materials have been utilized to fabricate sensors for VOCs detection, such as conjugating polymers [15,18,19], metal

* Corresponding author at: Department of Chemical and Materials Engineering, Chang Gung University, Taoyuan, 33302, Taiwan.
** Corresponding author at: Department of Electronic Engineering, Chang Gung University, Taoyuan, 33302, Taiwan.
E-mail addresses: mingchungwu@cgu.edu.tw (M.-C. Wu), cslai@mail.cgu.edu.tw (C.-S. Lai).

https://doi.org/10.1016/j.snb.2020.127760
Received 25 September 2019; Received in revised form 10 January 2020; Accepted 20 January 2020
Available online 22 January 2020
0925-4005/

oxides [20–23], organic/inorganic composites [24], and semiconductors quantum dot [25]. Among them, semiconducting quantum dots or rods are often fabricated with size from a few hundred to thousands of atoms depending on the manufacturing process. The versatile nanomaterials have broadband absorption [26], high photochemical stability [27], high quantum yields [28], and tunable sizes [29,30]. The tunable sizes or compositions feature [31] contributes to optoelectronic devices [32,33], luminescent solar concentrators [34,35], and sensors [36]. Aligning the quantum dots or rods could be a better indicator for gas sensors since the anisotropic nanocrystals perform a polarized light emission along their crystal long axis [37]. For instance, when CdSe nanoplatelets are oriented perpendicularly on the substrate, they have exhibited polarized light emission properties [38]. Vertically aligned thin ZnO nanorod arrays with diameters between 30–100 nm have shown excellent responses to H_2, NH_3, and CO exposure [39]. Ethanol sensing has also been investigated by ZnO nanowires up to 200 ppm at 300 °C [40]. For the detection of oxygen, the film thickness of the CdSe/CdS sensor has dominated the sensitivity in the measurements [41].

Moreover, the nano-sized sensing materials have been made for achieving high sensitivity due to the large surface area [42,43]. CdSe nanocrystals incorporated into PMMA polymer thin films have been monitored by the photoluminescence (PL) in sensing triethylamine and benzylamine vapor. It responded reversibly and rapidly to environmental changes [44]. On the other hand, the electrospinning technique is one of the best methods for fabricating a large quantity of sub-micro scale fibers or nanoscale fibers [45,46]. Fabricating high-performance sensing materials by the electrospinning technique is a simple and economical process [47,48]. The 3D electrospun materials construct thin films with a larger specific surface area. In our previous study, P3HT/PMMA blending fibers detects many types of VOCs, including acetone, ethanol, chlorobenzene, o-xylene, and toluene [16]. Although the detection limits of acetone, o-xylene, and toluene achieved 500 ppm, the study still requires improvement to reach higher sensitivity for gases.

If the concentration of VOCs is between lower explosive limit (LEL) and upper explosive limit (UEL), fire or explosion may occur. Therefore, the fabrication of VOC sensor to detect the concentrations below LEL is imperative. In this study, we developed a highly sensitive CdSe-CdS/Ag/PMMA composite scaffold for the detection of VOCs. It takes the advantages of the distinct optical property of CdSe-CdS and Ag surface plasmon resonance. We adopted photoluminescence (PL) spectra and time-resolved photoluminescence (TRPL) spectra to give an insight into the amplification of the response caused by the arrangement of the fiber and the addition of Ag NPs. Moreover, we collected the extinction spectra after every 30-degree rotation and found that the aligned CdSe-CdS/Ag/PMMA composite scaffold showed polarization-selective behavior, which resulted in the enhanced extinction change. The CdSe-CdS/Ag/PMMA composite scaffolds successfully achieved a non-selective detection limit of 500 ppm for chlorobenzene and 100 ppm for butanol.

2. Experimental details

2.1. Materials

PMMA (MW ~ 120,000 Da) was purchased from Sigma-Aldrich and used without further purification. CdSe-CdS was synthesized by a seeded growth approach [49]· To prepare Cd precursor solution I, 3.000 g of trioctylphosphine oxide (TOPO), 0.280 g of octadecylphosphonic acid (ODPA) and 0.060 g of CdO were well mixed in a glass flask at 150 °C under vacuum for one hour. For the preparation of CdSe seeds solution, 1.860 g of trioctylphosphine (TOP) and 0.058 g of Se were added into Cd precursor solution I at 370 °C under N_2 atmosphere for 3 min. To prepare Cd precursor solution II, 0.057 g of CdO was mixed with 3.000 g of TOPO, 0.290 g of ODPA, and 0.080 g of hexylphosphonic acid (HPA) at 350 °C under N_2 atmosphere in another glass flask. 0.120 g of sulfur was dissolved in 1.500 g of TOP and Cd precursor solution II. After 8 min of rigorous stirring, 200 µL of CdSe seeds solution was injected into the as-prepared solution. The CdSe-CdS core-shell quantum rods were prepared. For the preparation of Ag NPs, the synthesis method was referenced by a method published by C. Shen et al. [50]. 0.6 mmol of silver nitrate ($AgNO_3$) and 6.0 mmol of oleylamine were mixed in chlorobenzene (99.8 %, Acros) for one hour at 120 °C under N_2 atmosphere. The synthetic diameter of Ag NPs is ~17 nm on average.

2.2. Fabrication of CdSe-CdS/Ag/PMMA composite scaffold

The CdSe-CdS core-shell quantum rods were mixed into the stirred solution of PMMA in chlorobenzene. The concentration of the CdSe-CdS/PMMA blending solution was 27.0 wt%. Then, 1.0 wt% Ag NPs in chlorobenzene was added to CdSe-CdS/PMMA blending solution with continuous stirring for 24 h. The electrospinning device includes a high-voltage power supply (SC-PME50, Global Co. Ltd., Taiwan), a syringe pump (KDS-100, KD Scientific Inc., United States), and a grounded rotary collector with a diameter of 15.0 cm and a length of 15.0 cm (FES-COS, Falco Tech Enterprise Co. Ltd., Taiwan). The maximum voltage of the voltage power supply is 50.0 kV with a controlled 1.0 V resolution. The flow rates and volumes of the solution were automatically controlled by the syringe pump, which can handle various syringes with different quantities and needle sizes. The rotational speed of the metal collector was precisely controlled. With well-defined processing parameters of electrospinning, the CdSe-CdS/Ag/PMMA composite scaffolds were prepared on the glass substrate successfully. Generally, the applied voltage was scanned from 10.0 to 25.0 kV; the tip-to-collector distance was 10.0 cm; the rotational speed of the metal collector was 500 rpm; the flow rate of CdSe-CdS/Ag/PMMA precursor solution was 0.5 ml/h.

2.3. Characterizations

The microstructures of the sensing material with various PMMA fibers were observed using scanning electron microscopy (SEM, SNE-4500 M, SEC CO. Ltd., Korea) operated at an accelerating voltage of 15.0 kV. Spherical-aberration corrected field emission transmission electron microscope (JEOL, JEM-ARM200FTH, Japan) was used to observe the microstructures of CdSe-CdS quantum rods. UV–vis absorption spectra of CdSe-CdS quantum rods and extinction spectra of the CdSe-CdS/Ag/PMMA composite scaffold were measured by a UV–vis spectrophotometer V-730, Jasco International Co., Japan in the wavelength range of 400 to 1100 nm. For the photoluminescence PL measurement, the samples were excited with a 440 nm continuous-wave diode laser PDLH-440-25, DongWoo Optron Co. Ltd. with a 550 nm long pass filter. The emission spectrum was collected and analyzed by a photomultiplier tube detector system (PDS-1, DongWoo Optron Co. Ltd.) and conventional photon-counting electronics using a monochromator (Monora 150i, DongWoo Optron Co. Ltd.). The transient time-resolved photoluminescence (TRPL) plots were recorded by a time-correlated single-photon counting (TCSPC) (WELLS-001 FX, DongWoo Optron. Ltd.) spectrometer operating at a frequency of 312.5 MHz with 2 µs duration.

For VOCs detection, the 80.0 cm^3 quartz chamber was used to simulate the VOC pollution environment. Various solvents, such as acetone, diethyl ether, tetrahydrofuran, chloroform, toluene, chlorobenzene, o-xylene, methanol, ethanol, propanol, isopropanol, and butanol were applied to test the sensing properties of CdSe-CdS/Ag/PMMA composite scaffold. To create a saturated vapor pressure of VOCs, an excess of solvent was dropped into the quartz chamber. When the solvent completely evaporated, the CdSe-CdS/Ag/PMMA composite scaffold was placed at the center of the quartz chamber for validation. UV–vis spectrometer was used to measure the extinction spectrum of

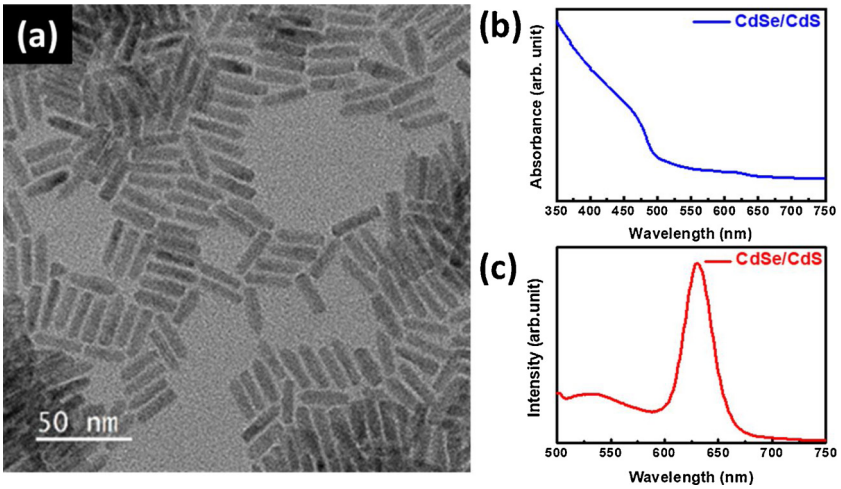

Fig. 1. (a) TEM image, **(b)** UV–vis spectrum and **(c)** PL spectrum of CdSe-CdS quantum rods.

the CdSe-CdS/Ag/PMMA composite scaffold versus ascending VOC exposure time. We also use gas chromatographs to establish calibration curves and confirm concentrations. The schematic of the CdSe-CdS/Ag/PMMA composite scaffold and the procedure of extinction spectra measurement are shown in Fig. S1. All the measurements were collected at 25 °C, 1.0 atm and under the relative humidity of 50 %. To avoid the disturbance of environmental moisture, we first defined a reasonable detection value where the response higher than 0.010. The value according to the maximum response of 0.005 tested with the humidity ranged from 33 % to 85 %.

3. Results and discussion

The synthesized core-shell CdSe-CdS quantum rods in this study showed distinct optical properties. In Fig. 1**a**, the microstructure of CdSe-CdS quantum rods were observed by the TEM, showing an average length of ~20.0 nm and an average diameter of ~5.0 nm. As shown in Fig. 1**b**, the band gaps calculated via UV–vis spectroscopy is 2.56 eV. The PL spectrum depicted the emission peak at 630 nm (Fig. 1**c**). Due to the outstanding optical properties of CdSe-CdS quantum rods, they were added into the electrospun PMMA fibers as a nanocomposite to enhance light harvesting for our sensing materials.

The applied voltage of electrospun was delicately controlled to vary the diameter of fibers. From the optical microscope images, we observed that the CdSe-CdS/PMMA nanocomposite seemed straight, but the diameters varied when the applied voltage was set at 10.0 kV (Fig. 2**a**). When the applied voltage was set at 15.0 kV, the CdSe-CdS/PMMA nanocomposite was slightly thinner, but the diameter varied between 1.0 and 4.0 μm (Fig. 2**b**). When the applied voltage was set at 20.0 kV, the diameter of CdSe-CdS/PMMA nanocomposite became even thinner and was more uniform at ~ 2.0 ± 0.3 μm (Fig. 2**c**). Unfortunately, when the applied voltage increased to 25.0 kV, the diameter of the CdSe-CdS/PMMA nanocomposite became thicker and nonuniform (Fig. 2**d**). The diameter size distribution of CdSe-CdS/PMMA nanocomposite fabricated with four applied voltage is plotted in Fig. 2**e**. Therefore, the CdSe-CdS/PMMA nanocomposite was prepared in the optimum condition by an applied voltage of 20.0 kV after considering the uniformity of the fibers.

The SPR of metal nanoparticles was used to enhance the detection limit of the sensing material. Ag NPs were used as a dopant in this study. The size of the synthesized Ag NPs was observed by TEM (Fig. 3**a**), and inset of Fig. 3**a** shows the high-magnification TEM image of Ag NPs. In Fig. 3**b**, the average particle size distribution of synthetic Ag NPs was summarized. The average size of Ag NPs observed was about 16.9 ± 0.7 nm. Fig. 3**c** depicts the absorption spectrum of

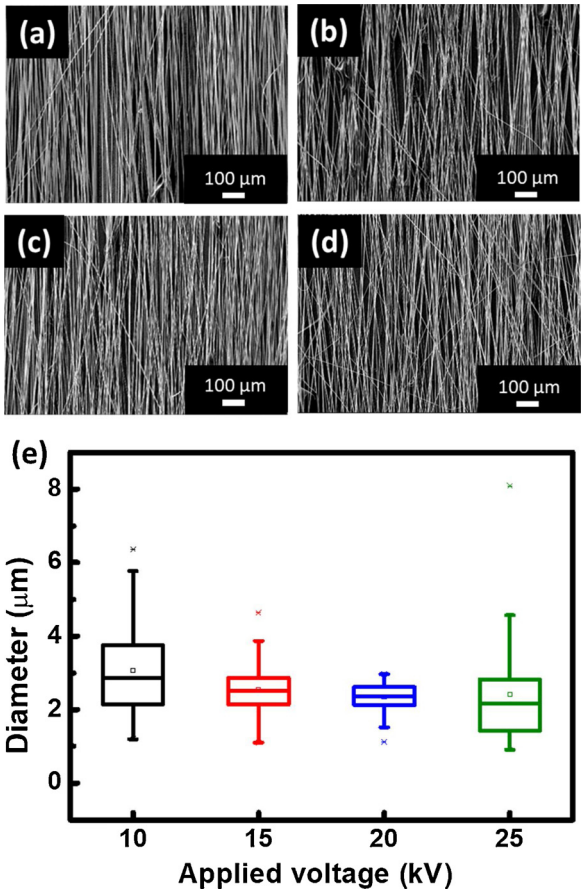

Fig. 2. The optical images of CdSe-CdS/PMMA nanocomposite fabricated at four different applied voltages, **(a)** 10.0 kV, **(b)** 15.0 kV, **(c)** 20.0 kV, and **(d)** 25.0 kV. **(e)** The plot of the diameter size distribution of CdSe-CdS/PMMA nanocomposite versus the applied electrospun voltage.

synthesized Ag NPs at around 430 nm. Ag NPs were then added into the CdSe-CdS/PMMA nanocomposites as a composite scaffold for higher VOCs response from SPR characteristics.

The UV-ozone etching technology was applied to generate more surface areas for VOCs acquisition. The equipment produces oxygen free radicals when the UV lamp irradiates oxygen molecules in the air. The oxygen-free radicals react with organic carbon chains on the surface of the CdSe-CdS/Ag/PMMA composite scaffold. Carbon monoxide

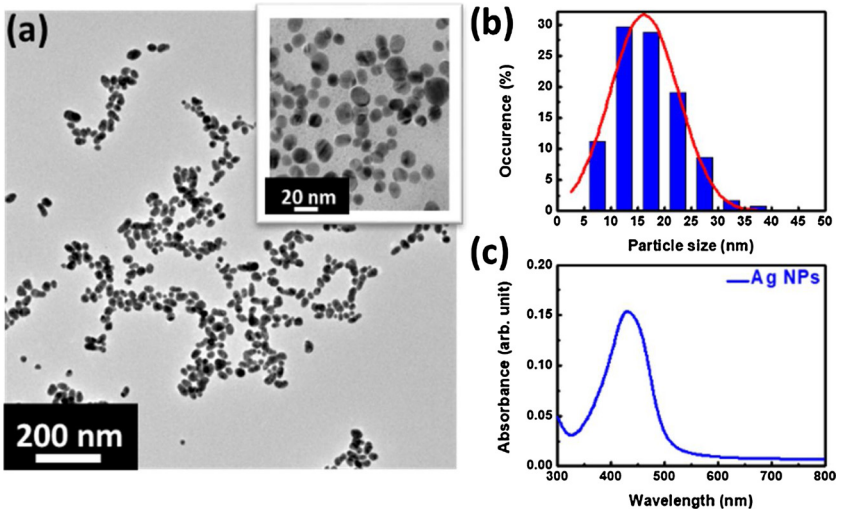

Fig. 3. (a) TEM image of Ag NPs. Inset photo is the high-magnification TEM image for the observation of individual Ag NP. **(b)** The relative particle numbers in sizes and its distribution, and **(c)** UV–vis absorbance spectrum of Ag NPs.

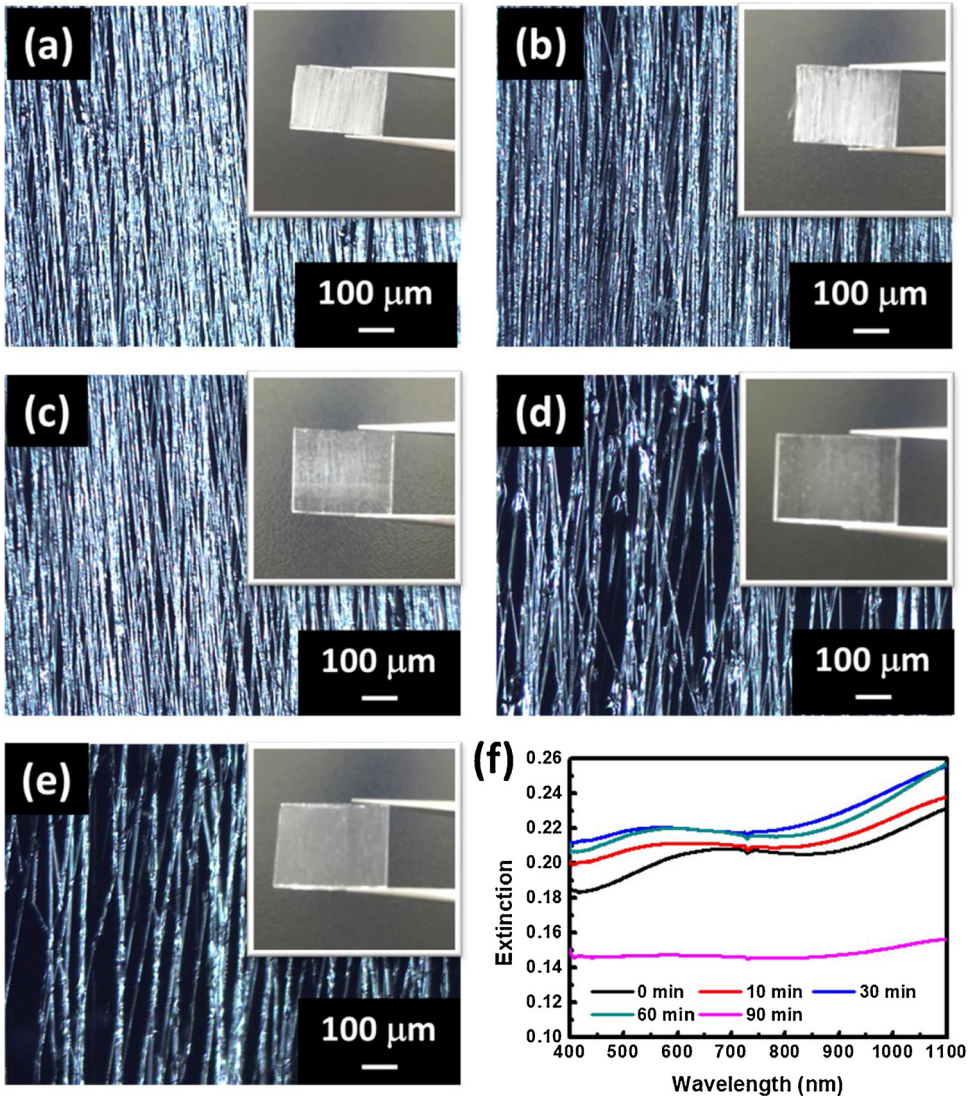

Fig. 4. The optical images of CdSe-CdS/Ag/PMMA composite scaffolds treated with UV-ozone etching after **(a)** 0 min, **(b)** 10 min, **(c)** 30 min, **(d)** 60 min, and **(e)** 90 min. The insets are the photographs of each sensing chip. **(f)** The extinction spectra of CdSe-CdS/Ag/PMMA composite scaffolds with various etching time.

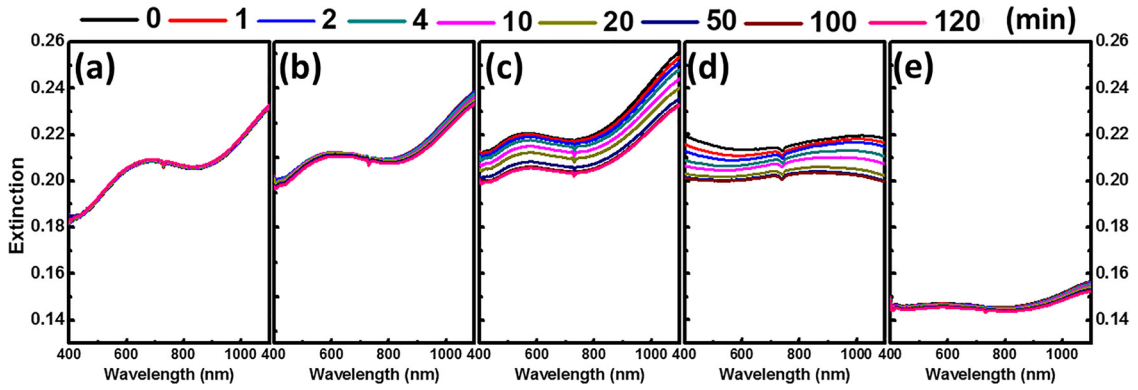

Fig. 5. The in-situ extinction spectra of **(a)** 0 min, **(b)** 10 min, **(c)** 30 min, **(d)** 60 min, and **(e)** 90 min UV-ozone etched CdSe-CdS/Ag/PMMA composite scaffolds when they were exposed to 10,000 ppm chlorobenzene.

was formed and was taken away by the outlet air flux. The UV-ozone treated surface of the CdSe-CdS/Ag/PMMA composite scaffold was observed using an optical microscope. It is noted that the surface of the CdSe-CdS/Ag/PMMA composite scaffold was gradually eroded concerning the etching time. The scaffold surface remained the same in the first 30 min of the etching time (Fig. 4**a**–**c**). When the etching time reached 60 min (Fig. 4**d**), the surface of the CdSe-CdS/Ag/PMMA composite scaffold has been significantly eroded. In Fig. 4**e**, the surface of the CdSe-CdS/Ag/PMMA composite scaffold has been etched away after 90 min. The extinction spectra of every individually etched sensing scaffold were ready to be investigated further for the in-situ VOCs sensing (Fig. 4**f**).

Every UV-ozone etched CdSe-CdS/Ag/PMMA composite scaffold was exposed to 10,000 ppm chlorobenzene vapor. Chlorobenzene is a common colorless flammable solvent and widely used as an intermediate to synthesize other chemicals. Fig. 5 shows the extinction spectra of UV-ozone etching treated CdSe-CdS/Ag/PMMA composite scaffolds in 0, 10, 30, 60, and 90 min. In Fig. 5**a**, the non UV-ozone etched CdSe-CdS/Ag/PMMA composite scaffold showed no apparent difference in chlorobenzene vapor. The extinction change of the CdSe-CdS/Ag/PMMA composite scaffold became stronger after 10 min of UV-ozone etching time (Fig. 5**b**). Minor changes in the composite scaffolds were observed. With 30 min of UV-ozone etching (Fig. 5**c**), the CdSe-CdS/Ag/PMMA composite scaffolds had noticeable variations in extinction spectra because of the rough surface of nanocomposite scaffold was able to absorb more chlorobenzene vapor than untreated surface sensing specimen. The 60 min UV-ozone etched CdSe-CdS/Ag/PMMA composite scaffolds exhibited the most significant extinction change (Fig. 5**d**). However, for the 90 min UV-ozone etched CdSe-CdS/Ag/PMMA composite scaffold, most of the nanocomposite scaffold has been removed by the vapor of chlorobenzene. The intensity of extinction was declined because the nanocomposite scaffolds have been over-etched. The variation of the extinction spectra becomes limited.

The nanocomposite scaffolds were measured by PL and TRPL to examine Ag doping effect on the nanocomposite scaffold. Fig. 6**a** shows the PL spectra of the CdSe-CdS/PMMA nanocomposites and the CdSe-CdS/Ag/PMMA composite scaffolds with electrospun fibers in either aligned or random orientation. The nanocomposites with Ag doping exhibited a high PL quenching because Ag NPs trapped the excited electrons from CdSe-CdS quantum rods. Hence, the Ag doping nanocomposites showed lower radiative recombination. Besides, the aligned nanocomposites demonstrated lower PL intensity than randomly orientated nanocomposites. These results indicated that the aligned fiber provides aisles for electron transport. We further measured the TRPL spectra of various nanocomposite scaffolds. In order to measure the fast charge carrier dynamics, the TRPL via the time-correlated single-photon counting was utilized. The fitting TRPL decay curves at 630 nm of the nanocomposite scaffolds are shown in Fig. 6**b**. The TRPL spectra

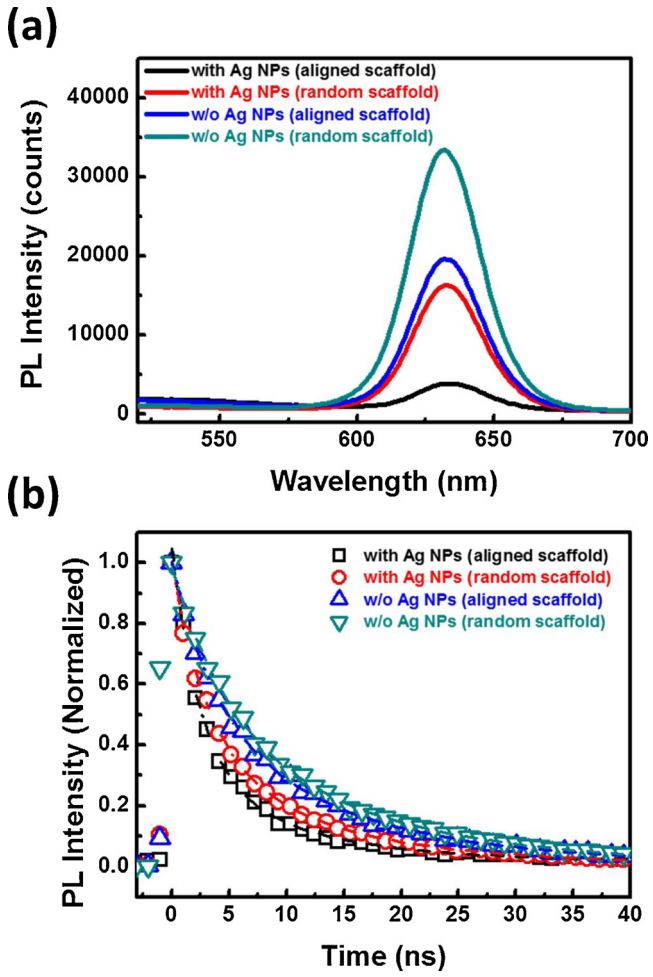

Fig. 6. (a) Photoluminescence spectra and **(b)** time-resolved photoluminescence spectra of the CdSe-CdS/PMMA nanocomposites and the CdSe-CdS/Ag/PMMA composite scaffolds with electrospun fibers of either aligned or random orientation.

were analyzed by the eliminated instrument response function bi-exponential decay kinetics. The data can be obtained by Eq. (1) [51].

$$\mathbf{F(t)} = A_1 exp\left(-\frac{t}{\tau_1}\right) + A_2 exp\left(-\frac{t}{\tau_2}\right) \quad (1)$$

The average lifetime was calculated by Eq. (2).

$$\tau_{avg} = \sum A_i \tau_i^2 / \sum A_i \tau_i \quad (2)$$

Table 1
Average lifetimes of the CdSe-CdS/PMMA nanocomposite and the CdSe-CdS/Ag/PMMA composite scaffolds with random/aligned arrangements.

Sample	Arrangement	A_1 (%)	τ_1 (ns)	A_2 (%)	τ_2 (ns)	τ_{avg} (ns)
CdSe-CdS/PMMA	random	48.0	4.84	52.0	14.90	10.07
	aligned	48.1	3.71	51.9	13.50	8.81
CdSe-CdS/Ag/PMMA	random	58.6	3.03	41.4	11.50	6.52
	aligned	67.1	2.34	32.9	9.34	4.64

The average PL lifetimes of nanocomposite scaffolds are shown in Table 1. The nanocomposite scaffolds with Ag doping exhibited lower PL lifetime. The best average PL lifetime of the CdSe-CdS/Ag/PMMA composite scaffolds was noticed at 4.64 ns. The results indicated that electron transport was increased with silver-containing in nanocomposite scaffolds.

The polarization properties of the aligned CdSe-CdS/Ag/PMMA composite scaffolds were measured in 10,000 ppm chlorobenzene too. The extinction spectra of the aligned CdSe-CdS/Ag/PMMA composite scaffolds were collected every 30 degrees at angles from 0 to 360 degrees (Fig. 7). It is noted the delta extinction that the sensing of chlorobenzene is fast within one minute. The CdSe-CdS/Ag/PMMA composite scaffold showed a high extinction change at 60° and 240°. These results suggest that CdSe-CdS quantum rods exhibited polarized emissions in the prepared composite scaffolds as a sensing signal. The delta extinction is saturated at 0.12 after the chlorobenzene exposure at 20 min. The aligned CdSe-CdS/Ag/PMMA composite scaffolds demonstrated a useful sensing device in a very short amount of time under a high concentration of chlorobenzene vapor. Moreover, various VOCs at 10,000 ppm were evaluated for CdSe-CdS/Ag/PMMA composite scaffolds. To quantify the response of VOCs, the band intensity at a wavelength of 572 nm was selected as an indicator. The Response_{572} was defined as below,

$$\Delta E = E_{0(572)} - E_{t(572)} \tag{3}$$

$$\text{Response}_{572} = \frac{\Delta E}{E_{0(572)}} \tag{4}$$

The CdSe-CdS/Ag/PMMA composite scaffolds were inserted into a quartz container and were exposed to various VOCs with different concentrations for 2 h. VOC vapor was adsorbed on the surface of CdSe-CdS/Ag/PMMA composite scaffold. This phenomenon causes changes in the extinction spectrum. In order to increase the detection accuracy and to minimize the effect of environmental humidity, we measured the response of CdSe-CdS/Ag/PMMA sensing material at 25 °C under various humidity as a control. The tested humidity ranged from 33 % to 85 % (Fig. S2). According to the response plot, if the response higher than 0.010, we defined it as an effective detection value. After that, we divided VOCs testing into two groups, the typical VOCs and alcoholic solvents. For typical VOCs, we adopted acetone, diethyl ether, tetrahydrofuran, chloroform, toluene, chlorobenzene, and o-xylene; for ordinary alcoholic solvents, we adopted methanol, ethanol, propanol, isopropanol, and butanol. The response plots and response time of the CdSe-CdS/Ag/PMMA composite scaffold are shown in Fig. 8 and Table 2, respectively. In Fig. 8**a**, the CdSe-CdS/Ag/PMMA composite scaffold sensing materials in chlorobenzene vapor showed the maximum distinguished response (~2 min). In Fig. 8**b**, the response time of alcoholic solvents depends on the methyl chain length of alcohol. The sensing material under butanol environment shows the fast response time (< 1 min) due to its hydrophilicity toward PMMA materials. The Response_{572} for butanol vapor is 0.45 with respect to the 0.15 for propanol and isopropanol.

Among all the concerns with VOCs, we concern the most about the leakage of VOCs in their normal usage. Thus, the detection of low concentration VOCs becomes very important. Herein, chlorobenzene and butanol vapor was detected from low to high concentrations as examples. Fig. 9 shows the sensing response of chlorobenzene and butanol at various concentrations. The response of the CdSe-CdS/Ag/PMMA composite scaffold became more significant as the VOC concentrations increased. The LEL is the minimum VOC vapor concentration to trigger the combustion in air. When the concentration of VOCs vapor is lower than the LEL, it is too lean to burn out the air [52]. The CdSe-CdS/Ag/PMMA composite scaffold was able to effectively detect VOC concentration that was much lower than the LEL. The LEL of chlorobenzene and butanol are 13,000 and 17,000 ppm, respectively. According to the effective detection value of R_{572} at 0.010, the detection limits of the CdSe-CdS/Ag/PMMA composite scaffold were able to reach 500 ppm for chlorobenzene and 100 ppm for butanol. The developed CdSe-CdS/Ag/PMMA composite scaffold in this study could achieve an instant responsive device to detect leakage of VOCs. This VOC device with a fast response time can prevent the industrial accident. However, permissible exposure concentration in the working

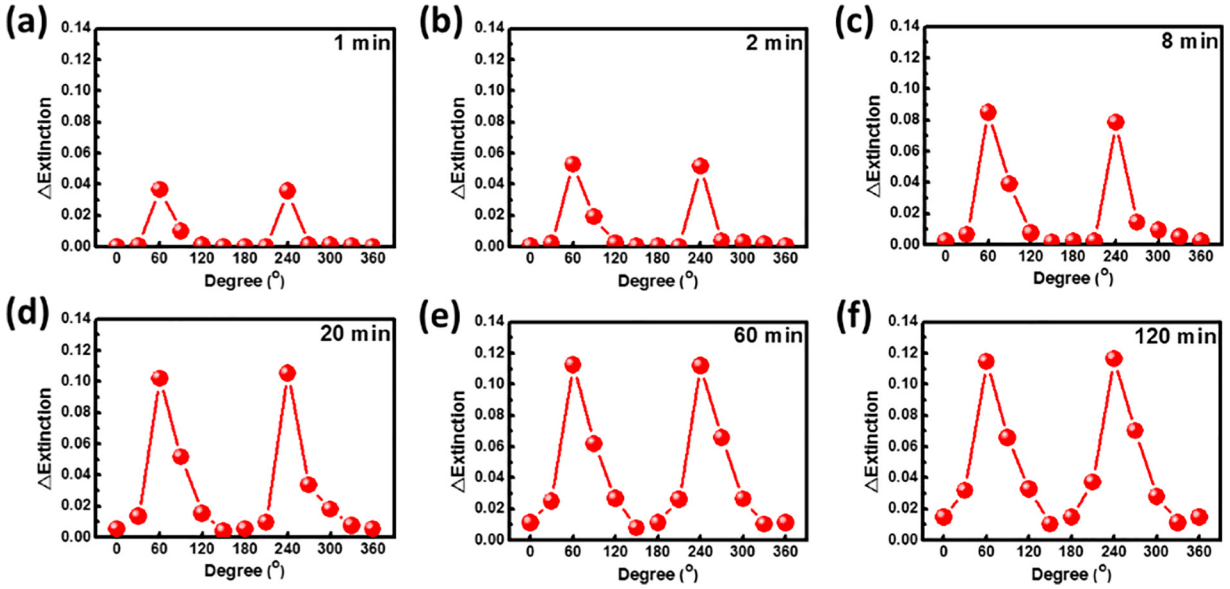

Fig. 7. The extinction change of CdSe-CdS/Ag/PMMA composite scaffolds measured in various polarization angles. These composite scaffolds were exposed to 10,000 ppm chlorobenzene for **(a)** 1 min, **(b)** 2 min, **(c)** 8 min, **(d)** 20 min, **(e)** 60 min, and **(f)** 120 min.

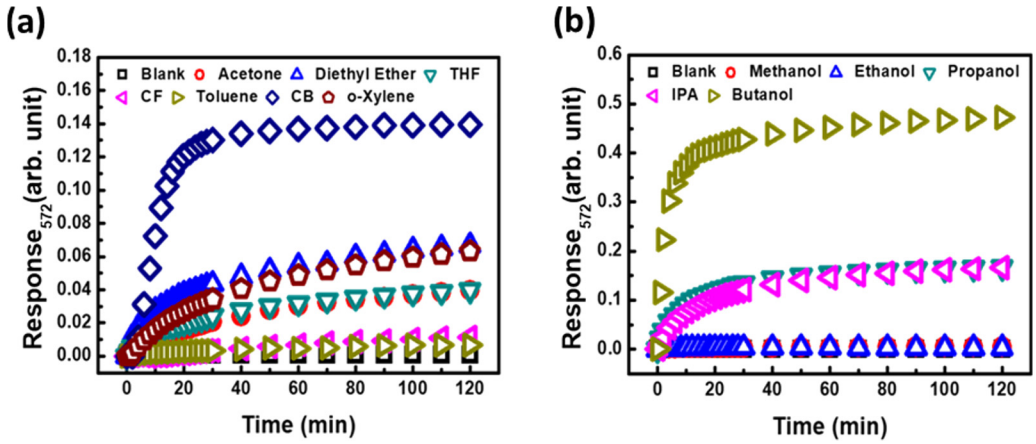

Fig. 8. The response plots of the CdSe-CdS/Ag/PMMA composite scaffold when it is exposed to 10,000 ppm of **(a)** typical VOCs and **(b)** alcoholic solvents.

Table 2
The response time of the CdSe-CdS/Ag/PMMA composite scaffold when it is exposed to 10,000 ppm of VOCs.

Type of VOCs	Response Time (min)
Blank	N/A
Acetone	12
Diethyl ether	2
Tetrahydrofuran (THF)	6
Chloroform (CF)	80
Toluene	16
Chlorobenzene (CB)	2
o-Xylene	6
Methanol	N/A
Ethanol	N/A
Propanol	1
Isopropanol	1
Butanol	< 1

environment is quite low. We listed the labor safety regulations of various countries for permissible exposure concentration in Table S1. Therefore, the development of low-cost, high-sensitivity, and real-time detection VOC sensors is the focus of future research.

4. Conclusion

In summary, the VOCs sensing materials consisting of CdSe-CdS/Ag/PMMA composite scaffolds were prepared successfully by the electrospinning process and UV-ozone etching treatment. A series of typical VOCs and alcoholic solvents were chosen to test the ultra-sensitivity of the CdSe-CdS/Ag/PMMA composite scaffold. The CdSe-CdS/Ag/PMMA composite scaffold could effectively detect the VOCs well below the lowest explosion limits within one minute. It even achieved a non-selective detection limit of 500 ppm for chlorobenzene and 100 ppm for butanol. This CdSe-CdS/Ag/PMMA composite scaffold enhances the progressing of VOCs sensing technology.

Declaration of Competing Interest

The authors declare that they have no known competing financial interests or personal relationships that could have appeared to influence the work reported in this paper.

Acknowledgments

The authors appreciate Dr. Ming-Tao Lee (BL-13A1) and Dr. Jyh-Fu Lee (BL-17C1) at National Synchrotron Radiation Research Centre for useful discussion and suggestions. The financial support from Ministry of Science and Technology of Taiwan (Project nos. 106-2221-E-182-057-MY3 and 108-2218-E-182-002), Industrial Technology Research Institute, Chang Gung University (QZRPD181), and Chang Gung Memorial Hospital, Linkou (CMRPD2H0172 and BMRPC74) is highly appreciated.

Appendix A. Supplementary data

Supplementary material related to this article can be found, in the online version, at doi:https://doi.org/10.1016/j.snb.2020.127760.

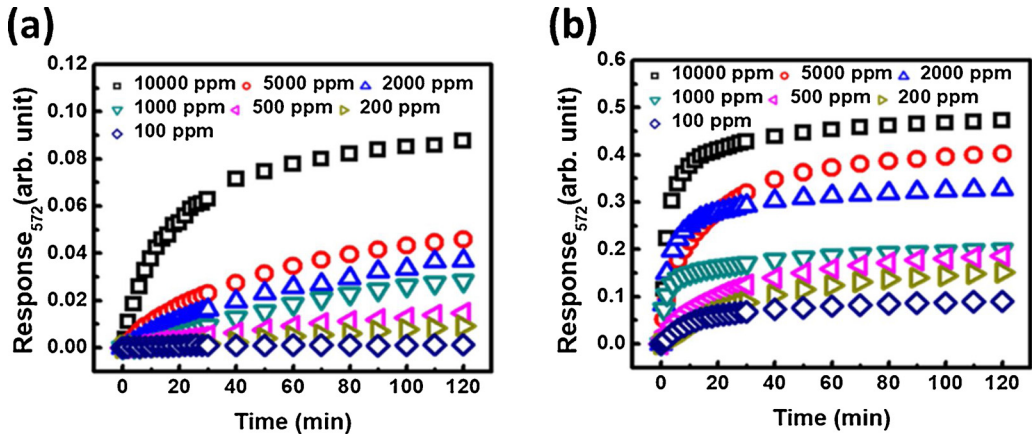

Fig. 9. Extinction change plot of CdSe-CdS/Ag/PMMA composite scaffolds exposed to **(a)** chlorobenzene and **(b)** butanol with various concentrations ranging from 100 to 10,000 ppm.

References

[1] Y. Bao, P. Xu, S. Cai, H. Yu, X. Li, Detection of volatile-organic-compounds (VOCs) in solution using cantilever-based gas sensors, Talanta 182 (2018) 148–155.
[2] A.H. Jalal, F. Alam, S. Roychoudhury, Y. Umasankar, N. Pala, S. Bhansali, Prospects and challenges of volatile organic compound sensors in human healthcare, ACS Sens. 3 (2018) 1246–1263.
[3] W. Geng, S. Ge, X. He, S. Zhang, J. Gu, X. Lai, H. Wang, Q. Zhang, Volatile organic compound gas-sensing properties of bimodal porous α-Fe_2O3 with ultrahigh sensitivity and fast response, ACS Appl. Mater. Interfaces 10 (2018) 13702–13711.
[4] T.M. Perfecto, C.A. Zito, T. Mazon, D.P. Volanti, Flexible room-temperature volatile organic compound sensors based on reduced graphene oxide–WO_3·0.33H_2O nanoneedles, J. Mater. Chem. C 6 (2018) 2822–2829.
[5] J. Tang, J. Fang, Y. Liang, B. Zhang, Y. Luo, X. Liu, Z. Li, X. Cai, J. Xian, H. Lin, W. Zhu, H. Guan, H. Lu, J. Zhang, J. Yu, Z. Chen, All-fiber-optic voc gas sensor based on side-polished fiber wavelength selectively coupled with cholesteric liquid crystal film, Sens. Actuators B 273 (2018) 1816–1826.
[6] H. Liu, Y. He, K. Nagashima, G. Meng, T. Dai, B. Tong, Z. Deng, S. Wang, N. Zhu, T. Yanagida, X. Fang, Discrimination of vocs molecules via extracting concealed features from a temperature-modulated p-type nio sensor, Sens. Actuators B 293 (2019) 342–349.
[7] M. Paknahad, C. McIntosh, M. Hoorfar, Selective detection of volatile organic compounds in microfluidic gas detectors based on “like dissolves like, Sci. Rep. 9 (2019) 161.
[8] J.-H. Kim, J.-H. Lee, Y. Park, J.-Y. Kim, A. Mirzaei, H.W. Kim, S.S. Kim, Toluene- and benzene-selective gas sensors based on pt- and pd-functionalized zno nanowires in self-heating mode, Sens. Actuators B 294 (2019) 78–88.
[9] I. Constantinoiu, C. Viespe, Detection of volatile organic compounds using surface acoustic wave sensor based on nanoparticles incorporated in polymer, Coatings 9 (2019) 373.
[10] A. Dey, Semiconductor metal oxide gas sensors: a review, Mater. Sci. Eng. B 229 (2018) 206–217.
[11] S. Zhang, Y. Zhao, X. Du, Y. Chu, S. Zhang, J. Huang, Gas sensors based on nano/microstructured organic field-effect transistors, Small 15 (2019) 1805196.
[12] I. Constantinoiu, D. Miu, C. Viespe, Surface acoustic wave sensors for ammonia detection at room temperature based on SnO_2/Co_3O_4 bilayers, J. Sens. 2019 (2019) 6.
[13] K. Haddad, A. Abokifa, S. Kavadiya, B. Lee, S. Banerjee, B. Raman, P. Banerjee, C. Lo, J. Fortner, P. Biswas, SnO_2 nanostructured thin films for room-temperature gas sensing of volatile organic compounds, ACS Appl. Mater. Interfaces 10 (2018) 29972–29981.
[14] H. Fan, S. Han, Z. Song, J. Yu, H.E. Katz, Organic field-effect transistor gas sensor based on go/pmma hybrid dielectric for the enhancement of sensitivity and selectivity to ammonia, Org. Electron. 67 (2019) 247–252.
[15] H.-C. Liao, C.-P. Hsu, M.-C. Wu, C.-F. Lu, W.-F. Su, Conjugated polymer/nanoparticles nanocomposites for high efficient and real-time volatile organic compounds sensors, Anal. Chem. 85 (2013) 9305–9311.
[16] M.-C. Wu, S.-H. Chan, T.-F. Lin, C.-F. Lu, W.-F. Su, Detection of volatile organic compounds using electrospun P3HT/PMMA fibrous film, J. Taiwan Inst. Chem. Eng. 78 (2017) 552–560.
[17] S.-H. Chan, T.-F. Lin, M.-C. Wu, S.-H. Chen, W.-F. Su, C.-S. Lai, Using aligned poly (3-hexylthiophene)/poly(methyl methacrylate) blend fibers to detect volatile organic compounds, Jpn. J. Appl. Phys. 57 (2018) 04FM06.
[18] V.C. Gonçalves, B.M. Nunes, D.T. Balogh, C.A. Olivati, Detection of volatile organic compounds using a polythiophene derivative, Phys. Status Solidi A 207 (2010) 1756–1759.
[19] H. Bai, G. Shi, Gas sensors based on conducting polymers, Sensors 7 (2007) 267.
[20] A. Mirzaei, S.G. Leonardi, G. Neri, Detection of hazardous volatile organic compounds (VOCs) by metal oxide nanostructures-based gas sensors: a review, Ceram. Int. 42 (2016) 15119–15141.
[21] S.-Y. Cho, H.-W. Yoo, J.Y. Kim, W.-B. Jung, M.L. Jin, J.-S. Kim, H.-J. Jeon, H.-T. Jung, High-resolution p-type metal oxide semiconductor nanowire array as an ultrasensitive sensor for volatile organic compounds, Nano Lett. 16 (2016) 4508–4515.
[22] N. Mahapatra, A. Ben-Cohen, Y. Vaknin, A. Henning, J. Hayon, K. Shimanovich, H. Greenspan, Y. Rosenwaks, Electrostatic selectivity of volatile organic compounds using electrostatically formed nanowire sensor, ACS Sens. 3 (2018) 709–715.
[23] A. Henning, N. Swaminathan, Y. Vaknin, T. Jurca, K. Shimanovich, G. Shalev, Y. Rosenwaks, Control of the intrinsic sensor response to volatile organic compounds with fringing electric fields, ACS Sens. 3 (2018) 128–134.
[24] Y. Qin, J. Shi, X. Gong, Z. Tian, P. Zhang, J. Lu, A luminescent inorganic/organic composite ultrathin film based on a 2D cascade fret process and its potential voc selective sensing properties, Adv. Funct. Mater. 26 (2016) 6752–6759.
[25] H. Liu, W. Shen, X. Chen, A room temperature operated ammonia gas sensor based on ag-decorated TiO_2 quantum dot clusters, RSC Adv. 9 (2019) 24519–24526.
[26] Y. Fang, K. Wang, D. Hui, F. Xu, W. Liu, S. Yang, L. Wang, Monitoring of seawater immersion degradation in glass fibre reinforced polymer composites using quantum dots, Compos. B Eng. 112 (2017) 93–102.
[27] M. Frasco, N. Chaniotakis, Semiconductor quantum dots in chemical sensors and biosensors, Sensors 9 (2009) 7266.
[28] T.V. Duncan, M.A. Méndez Polanco, Y. Kim, S.-J. Park, Improving the quantum yields of semiconductor quantum dots through photoenhancement assisted by reducing agents, J. Phys. Chem. C 113 (2009) 7561–7566.
[29] J. Zhou, Y. Liu, J. Tang, W. Tang, Surface ligands engineering of semiconductor quantum dots for chemosensory and biological applications, Mater. Today 20 (2017) 360–376.
[30] Y. Yang, H.-Q. Shi, W.-N. Li, H.-M. Xiao, Y.-S. Luo, S.-Y. Fu, T. Liu, Tunable photoluminescent properties of novel transparent CdSe-QD/silicone nanocomposites, Compos. Sci. Technol. 71 (2011) 1652–1658.
[31] J.X. Wang, X.W. Sun, Y. Yang, H. Huang, Y.C. Lee, O.K. Tan, L. Vayssieres, Hydrothermally grown oriented ZnO nanorod arrays for gas sensing applications, Nanotechnology 17 (2006) 4995.
[32] A.A. Chistyakov, M.A. Zvaigzne, V.R. Nikitenko, A.R. Tameev, I.L. Martynov, O.V. Prezhdo, Optoelectronic properties of semiconductor quantum dot solids for photovoltaic applications, J. Phys. Chem. Lett. 8 (2017) 4129–4139.
[33] X. Gong, L. Pan, C.Y. Tang, L. Chen, Z. Hao, W.-C. Law, X. Wang, C.P. Tsui, C. Wu, Preparation, optical and thermal properties of CdSe–ZnS/poly(lactic acid) (PLA) nanocomposites, Compos. B Eng. 66 (2014) 494–499.
[34] F. Meinardi, S. Ehrenberg, L. Dhamo, F. Carulli, M. Mauri, F. Bruni, R. Simonutti, U. Kortshagen, S. Brovelli, Highly efficient luminescent solar concentrators based on earth-abundant indirect-bandgap silicon quantum dots, Nat. Photonics 11 (2017) 177.
[35] D.I. Son, H.Y. Yang, T.W. Kim, W.I. Park, Transparent and flexible ultraviolet photodetectors based on colloidal ZnO quantum dot/graphene nanocomposites formed on poly(ethylene terephthalate) substrates, Compos. B Eng. 69 (2015) 154–158.
[36] Y. Lou, Y. Zhao, J. Chen, J.-J. Zhu, Metal ions optical sensing by semiconductor quantum dots, J. Mater. Chem. C 2 (2014) 595–613.
[37] Y. Gao, V.D. Ta, X. Zhao, Y. Wang, R. Chen, E. Mutlugun, K.E. Fong, S.T. Tan, C. Dang, X.W. Sun, H. Sun, H.V. Demir, Observation of polarized gain from aligned colloidal nanorods, Nanoscale 7 (2015) 6481–6486.
[38] B. Abécassis, M.D. Tessier, P. Davidson, B. Dubertret, Self-assembly of CdSe nanoplatelets into giant micrometer-scale needles emitting polarized light, Nano Lett. 14 (2014) 710–715.
[39] J.X. Wang, X.W. Sun, Y. Yang, H. Huang, Y.C. Lee, O.K. Tan, L. Vayssieres, Hydrothermally grown oriented Zno nanorod arrays for gas sensing applications, Nanotechnology 17 (2006) 4995–4998.
[40] Q. Wan, Q.H. Li, Y.J. Chen, T.H. Wang, X.L. He, J.P. Li, C.L. Lin, Fabrication and ethanol sensing characteristics of Zno nanowire gas sensors, Appl. Phys. Lett. 84 (2004) 3654–3656.
[41] V.A. Smyntyna, V. Gerasutenko, S. Kashulis, G. Mattogno, S. Reghini, The causes of thickness dependence of cdse and cds gas-sensor sensitivity to oxygen, Sens. Actuators B 19 (1994) 464–465.
[42] C. Elosua, F.J. Arregui, I.D. Villar, C. Ruiz-Zamarreño, J.M. Corres, C. Bariain, J. Goicoechea, M. Hernaez, P.J. Rivero, A.B. Socorro, A. Urrutia, P. Sanchez, P. Zubiate, D. Lopez-Torres, N.D. Acha, J. Ascorbe, A. Ozcariz, I. Matias, Micro and nanostructured materials for the development of optical fibre sensors, Sensors 17 (2017) 2312.
[43] X.-J. Huang, Y.-K. Choi, Chemical sensors based on nanostructured materials, Sens. Actuators B 122 (2007) 659–671.
[44] A.Y. Nazzal, L. Qu, X. Peng, M. Xiao, Photoactivated cdse nanocrystals as nanosensors for gases, Nano Lett. 3 (2003) 819–822.
[45] C. Luo, X. Wang, J. Wang, K. Pan, One-pot preparation of polyimide/Fe_3O_4 magnetic nanofibers with solvent resistant properties, Compos. Sci. Technol. 133 (2016) 97–103.
[46] K. Bilge, E. Ozden-Yenigun, E. Simsek, Y.Z. Menceloglu, M. Papila, Structural composites hybridized with epoxy compatible polymer/MWCNT nanofibrous interlayers, Compos. Sci. Technol. 72 (2012) 1639–1645.
[47] B. Ding, M. Wang, X. Wang, J. Yu, G. Sun, Electrospun nanomaterials for ultrasensitive sensors, Mater. Today 13 (2010) 16–27.
[48] I.A.A. Terra, R.C. Sanfelice, G.T. Valente, D.S. Correa, Optical sensor based on fluorescent PMMA/PFO electrospun nanofibers for monitoring volatile organic compounds, J. Appl. Polym. Sci. 135 (2018) 46128.
[49] L. Carbone, C. Nobile, M. De Giorgi, F.D. Sala, G. Morello, P. Pompa, M. Hytch, E. Snoeck, A. Fiore, I.R. Franchini, M. Nadasan, A.F. Silvestre, L. Chiodo, S. Kudera, R. Cingolani, R. Krahne, L. Manna, Synthesis and micrometer-scale assembly of colloidal Cdse/Cds nanorods prepared by a seeded growth approach, Nano Lett. 7 (2007) 2942–2950.
[50] C. Shen, C. Hui, T. Yang, C. Xiao, J. Tian, L. Bao, S. Chen, H. Ding, H. Gao, Monodisperse noble-metal nanoparticles and their surface enhanced raman scattering properties, Chem. Mater. 20 (2008) 6939–6944.
[51] J. Zhang, X. Zhang, J.Y. Zhang, Size-dependent time-resolved photoluminescence of colloidal cdse nanocrystals, J. Phys. Chem. C 113 (2009) 9512–9515.
[52] https://www.mathesongas.com/pdfs/products/Lower-(LEL)-&-Upper-(UEL)-Explosive-Limits-.pdf.

Ming-Chung Wu received the M.S. and Ph.D. degrees from National Taiwan University, Taiwan, in 2004, 2008, respectively, both in materials science and engineering. In January 2012, He joined the faculty of Department of Chemical and Materials Engineering at Chang Gung University, Taiwan. Dr. Ming-Chung Wu’s research group develops innovative nanomaterials for various applications including photocatalysis, volatile organic compounds sensing devices, antimicrobial technology, flexible electronic.

Chih-Kunag Kao received the M.S. degree from Department of Chemical and Materials Engineering at Chang Gung University in 2017 with a research interest of developing VOCs sensing materials.

Tz-Feng Lin is an Assistant Professor in Department of Fiber and Composite Materials, Feng Chia University. He received his Ph.D degree from Department of Chemical Engineering at National Tsing Hua University in 2009. His main research interests focus

on a wide range of polymer-related research fields.

Shun-Hsiang Chan received the Ph.D. degree from Department of Chemical and Materials Engineering at Chang Gung University in 2018. His research interests are in developing perovskite solar cells and developing novel materials for VOCs sensors.

Shih-Hsuan Chen is now studying for his Ph.D degree at Department of Chemical and Materials Engineering at Chang Gung University with a research interest covering the production of sensors for the detection of VOCs and perovskite solar cells.

Chi-Hung Lin received the M.S. degree from Department of Chemical and Materials Engineering, Chang Gung University in 2018 with a research interest of developing VOCs sensor.

Yu-Ching Huang is an Assistant Professor in Department of Materials Engineering at Ming Chi University of Technology. He received the M.S. and Ph.D. degrees from National Taiwan University, Taipei, in 2005, 2010, respectively, both in materials science and engineering. His research interests focus on organic and perovskite solar cells, synchrotron radiation source analysis material structure technology.

Ziming Zhou is now studying for his Ph.D at Department of Electrical and Electronic Engineering at South University of Science and Technology of China with a research interest covering emiconductor nanocrystalline luminescent materials (quantum dots / rods, perovskite nanocrystals).

Kai Wang received the Ph.D. degree from School of Optoelectronics Science and Engineering, Huazhong University of Science in 2011. He is an Associate Professor in Department of Electrical and Electronic Engineering at South University of Science and Technology of China. His research interests focus on semiconductor nanocrystalline luminescent materials (quantum dots / rods, perovskite nanocrystals) and their optoelectronic devices (light-emitting diodes, photodetectors), new display (QLED, QD-MicroLED), semiconductor lighting research.

Chao-Sung Lai received the B.S. and Ph.D. degrees from National Chiao Tung University, Taiwan, in 1991 and 1996, respectively. He joined Chang Gung University as an Assistant Professor, where he has been a Full Professor since 2006 and has been the Dean of the Engineering of Chang Gung University since 2013. He has been engaged in the research of the characterization and reliability of MOSFETs, Flash memory, high-k dielectrics, metal gates, and biosensors.